Letter of Intent
Neutrino Oscillation Experiment at JHF

Summary

The first stage of a next-generation long baseline neutrino oscillation experiment is proposed to explore the physics beyond the Standard Model. The experiment will use the high intensity proton beam from the JHF 50 GeV proton synchrotron (JHF PS), and Super-Kamiokande as a far detector. The baseline length will be 295 km. The beam power of JHF PS is capable of delivering 3.3×10^{14} 50 GeV protons every 3.5 seconds (0.75 MW). The experiment assumes 130 days of operation at full intensity for five years. The high intensity neutrino beam is produced in an off-axis configuration. The peak neutrino energy is tuned to the oscillation maximum of $\sim$0.8 GeV to maximize the sensitivity to neutrino oscillations.

The merits of this experiment can be summarized as follows:

- The off-axis beam can produce the highest possible intensity with a narrow energy spread. The oscillation maximum will be $\sim$0.8 GeV for the distance of 295 km and $\Delta m^2 \sim 3 \times 10^{-3} eV^2$. The corresponding angle of the beam line axis relative to the direction of far detector is about 2 degrees.

- The far detector, Super-Kamiokande (SK), already exists. Experience in operating SK, including analysis tools, already exists. SK has excellent performance in detecting low-energy neutrinos.

- The neutrino events at sub-GeV are dominated by charged current quasi-elastic interactions, hence the neutrino energy E_ν can be reconstructed by two body kinematics.

The expected sensitivities in the first stage, assuming 0.75 MW and 130 days operation for five years are:

- Discovery of $\nu_\mu \rightarrow \nu_e$ at $\Delta m^2 \sim 3 \times 10^{-3} eV^2$ down to $sin^2 2\theta_{13} \sim 0.006$. This is a factor of twenty improvement in sensitivity over past experiments.

- Precision measurements of oscillation parameters in ν_μ disappearance down to $\delta(\Delta m^2_{23}) = 10^{-4}$ eV^2 and $\delta(\sin^2 2\theta_{23}) = 0.01$.

- Search for a sterile component in ν_μ disappearance by detecting neutral current events.

With successful completion of the first stage, a second stage of the experiment can be envisaged. In the second stage with the 1 Mt Hyper-Kamiokande detector and upgraded 4 MW PS, CP violation in the lepton sector can be probed, if $\sin^2 2\theta_{13}$ is in the discovery range of the first stage of the experiment. Sensitivity to proton decay is significantly extended up to 10^{35} ($(2 \sim 3) \times 10^{34}$) years lifetime for the $p \rightarrow e^+\pi^0$ ($p \rightarrow \bar{\nu} K^+$) mode.

Japan

KEK
Y. Hayato, A. K. Ichikawa, T. Ishida, T. Ishii, J. Kameda, T. Kobayashi, K. Nakamura, Y. Oyama, M. Sakuda, M. Tanaka, Y. Totsuka, M. Yoshida
ICRR, University of Tokyo
Y. Itow, T. Kajita, K. Kaneyuki, Y. Koshio, M. Miura, S. Moriyama, M. Nakahata, T. Namba, Y. Obayashi, C. Saji, M. Shiozawa, Y. Suzuki, Y. Takeuchi
Hiroshima University
I. Endo, M. Iinuma, T. Takahashi
Kobe University
S. Aoki, T. Hara, A. Suzuki
Kyoto University
T. Nakaya, K. Nishikawa
Miyagi University of Education
Y. Fukuda
Osaka City University
T. Okusawa, K. Yamamoto
Tohoku University
T. Hasegawa, K. Inoue, M. Koga, J. Shirai, F. Suekane, A. Suzuki
University of Tokyo
H. Aihara, M. Iwasaki, M. Yokoyama

Canada

University of Alberta
P. Kitching, J. McDonald, M. Vincter
University of Regina
R. Tacik
University of Toronto
J. Martin
TRIUMF
M. Barnes, E. Blackmore, J. Doornbos, P. Gumplinger, R. Helmer, R. Henderson, A. Konaka, G. Marshall, J. Macdonald, J.M. Poutissou, G. Wait, S. Yen
University of Victoria
R. Kowalewski
York University
S. Bhadra, S. Menary

France

CEA SACLAY - DSM/DAPNIA - Service de Physique des particules
J. Bouchez, C. Cavata, J. Mallet, L. Mosca, F. Pierre

Italy

INFN - University of Bari
G. Catanesi, E. Radicioni
INFN - University of Napoli
V. Palladino
INFN - University of Padova
M. Mezzetto
INFN - University of Roma
U. Dore, P. Loverre, L. Ludovici

Korea

Kangwon University
S.K. Nam
Kyungpook National University
W. Kim
KyungSang National University
I.G. Park
Dongshin University
M.Y. Pac
SungKyunKwan University
Y.I. Choi
Seoul National University
S.B. Kim, K. Joo
Chonnam Naitonal University
J.Y. Kim, I.T. Lim
Yonsei University
Y. Kwon

Poland

Warsaw University
D. Kielczewska

Russia

Institute for Nuclear Research RAS
A.V. Butkevich, Yu.G. Kudenko, V.A. Matveev, S.P. Mikheyev

Spain

University of Barcelona
E. Fernandez, F. Sanchez
University of Valencia
J. Burguet, J.J. Gomez Cadenas, A. Tornero

Switzerland

University of Geneva
A. Blondel, S. Gilardoni

UK

Rutherford Appleton Laboratory
D.L. Wark
Imperial College London
P. Dornan, K. Long
Queen Mary Westfield College London
P. Harrison
University of Liverpool
J.B. Dainton, A. Mehta, C. Touramanis

USA

Argonne National Laboratory
M. Goodman
Boston University
E. Kearns, J.L. Stone, L.R. Sulak, C.W. Walter
Brookheavn National Laboratory
M. Goldhaber, M. Harrison, P. Wanderer
University of California, Berkeley and Lawrence Berkeley National Laboratory
K. M. Heeger, Kam-Biu Luk
University of California, Irvine
W.R. Kropp, S. Mine, M.B. Smy, H.W. Sobel, M.R. Vagins
California State University Dominguez Hills
K. Ganezer, J. Hill, W. Keig
University of Hawaii
J.G. Learned, S. Matsuno
Los Alamos National Laboratory
T.J. Haines
Louisiana State University
R. Svoboda
Massachusetts Institute of Technology
K. Scholberg
The University of Pennsylvania
E.W. Beier, W.J. Heintzelman, N. McCauley. S.M. Oser
The University of Rochester
A. Bodek, H. Budd, K. McFarland, P. Slattery, M. Zielinski
The State University of New York at Stony Brook
C.K. Jung, K. Kobayashi, C. McGrew, A. Sarrat, C. Yanagisawa
University of Washington
R.J. Wilkes

Contact Person : Koichiro Nishikawa (Kyoto University)
Email : nishikaw@scphys.kyoto-u.ac.jp, Tel : 81-75-753-3859

Contents

1 Physics goal of the JHF neutrino project

The main physics motivation of the JHF neutrino project is to explore physics at much higher energy scale than the electro-weak unification scale. Studies of atmospheric and solar neutrinos have shown that neutrinos have masses and have large mixings. The confirmation of the existence of neutrino oscillations by the first generation experiments must be followed by precision measurements of the neutrino oscillation parameters. Neutrino mass and mixing can be one of a few possible windows of physics near the Grand Unification energy scale. In addition, comparison of neutrino and anti-neutrino oscillations are the only possible way to search for leptonic CP violation with presently available technologies. A massive detector, which is essential to have enough statistics for neutrino physics, is also important for the search and studies of proton decay. Observation of proton decay would be direct evidence of quark and lepton unification. Together, baryon number and CP violation may lead us to the understanding of the baryon/anti-baryon asymmetry in the universe [1].

1.1 History

The neutrino program has been one of the main motivations of building a high intensity proton synchrotron since the JHF project was first proposed in 1995. The possible neutrino experiments were first discussed in 1996 at INS symposium, and at JAERI in 1997 at JAERI workshop. Due to rapid progress of neutrino physics in the world, it became necessary to re-evaluate the physics goals for the next generation neutrino oscillation experiment. The JHF neutrino experiment-working group was formed in 1999 to formulate our strategy. The results of the studies were reported at a workshop of the Japanese high-energy physicist community and the project received strong endorsement [2]. The Expression of Interest was submitted to the JHF project team in January 2000. The first LOI was published in 2001 [3]. In 2002, two international workshops were held. The attendants include physicists from Canada, France, Italy, Korea, Russia, Spain, UK and US, and an international working group has been formed. This LOI is a summary of the old LOI, updated to reflect recent developments.

1.2 Merits of the JHF physics program

The physics program consists of two distinct stages. This LOI is for the first stage of the program. The feasibility of the entire physics program depends on the results of the first stage. The JHF neutrino experiment (JHFnu) has the following merits.

- The far detector
  JHFnu will use the world largest water Čerenkov detector, Super-Kamiokande (SK), as the far detector in the initial stage. SK has excellent energy resolution and e/μ identification capability in low energy neutrino reactions, where the multiplicity of the final state particles is small.

- The neutrino beam energy
  The maximum sensitivity of the oscillation parameters can be achieved by tuning the neutrino beam energy to the oscillation maximum. The oscillation maximum will occur at a neutrino energy, E_ν, less than 1 GeV for the 295 km baseline with $\Delta m^2 \sim 3 \times 10^{-3}$ eV^2. This neutrino energy is well matched to the detector capability.

- E_ν reconstruction
  The charged current interaction is dominated by the quasi-elastic interaction (CCQE) below 1 GeV. This enable us to make a precision determination of the neutrino energy of both ν_μ and ν_e. The energy can be calculated by a formula:

$$E_\nu = \frac{m_N E_l - m_l^2/2}{m_N - E_l + p_l cos\theta_l}, \quad (1)$$

  where m_N and m_l are the masses of the neutron and lepton (=e or μ), E_l, p_l and θ_l are the energy, momentum, and angle of the lepton relative to the neutrino beam, respectively.

- Off-axis beam
  The precision of the oscillation parameters is limited mainly due to the high-energy components. The inelastic reactions of high-energy neutrinos constitute the backgrounds to neutrino energy measurements with the CCQE. In addition, the inelastic reactions produce π^0s that are the main background for electron appearance search. The experiment will use an off-axis beam to accomplish the highest possible intensity of low energy neutrinos with only a small high-energy tail in the spectrum.

- Start up of the experiment
  SK has been in operation for many years and the relevant software already exists. The intensity of the low energy neutrino beam is proportional to the proton beam power and does not require a specific proton energy in the initial operation of the accelerator. The experiment will be able to accommodate any reasonable start-up scenario of the accelerator, and can produce physics results in a short time after initial operation.

1.3 The present understanding of neutrino mass and mixing

The recent progress of neutrino physics and expected one in the near future can be summarized as follow. In the three-neutrino scheme, the neutrino oscillation can be described by five parameters: three mixing angles $\theta_{12}, \theta_{23}, \theta_{13}$ between weak eigen-state and mass eigen-states, one CP-violating phase δ, and two independent mass squared differences, $\Delta m^2_{21} (= m_2^2 - m_1^2)$ and $\Delta m^2_{32} (= m_3^2 - m_2^2)$ with $\Delta m^2_{31} = \Delta m^2_{32} - \Delta m^2_{21}$ [4] [5]. There are two strong evidences for neutrino oscillation and one other result remains to be examined.

1. Oscillation of $\nu_\mu \to \nu_\tau$ with $\Delta m^2 \sim 3 \times 10^{-3}$ eV^2 (Δm^2_{23})

   - The SK collaboration [6] showed that the rate of upward-going ν_μ is about one-half of that expected. The corresponding oscillation parameters are 1.6×10^{-3} eV^2 $< \Delta m^2 <$ 3.9×10^{-3} eV^2, $\sin^2 2\theta > 0.92$ at 90% CL.
   - The K2K collaboration [7] showed a reduction of ν_μ flux with more than 99% confidence level. The results also show indication of energy spectrum distortion during the 250 km flight path from KEK to Kamioka. The resultant oscillation parameters are consistent with the atmospheric neutrino observation. If confirmed with more statistics, this is direct evidence of neutrino oscillation in ν_μ disappearance at $\Delta m^2 \sim$ (a few) $\times 10^{-3}$ eV^2.

- The most likely source of the ν_μ rate reduction is due to $\nu_\mu \to \nu_\tau$ oscillation, based on the atmospheric neutrino observations in SK [8]. Confirmation can be expected by the CERN-Gran-Sasso project, by identifying the production of tau leptons.

2. Oscillation $\nu_e \to \nu_\tau$ and $\to \nu_\mu$ with $\Delta m^2 \sim 10^{-4}$ eV^2 mass region (Δm^2_{12})

   - The SNO [9] collaboration announced their results of solar neutrino (ν_e) observation. The results show ν_μ and/or ν_τ components exist in the solar neutrinos. This is direct evidence of neutrino oscillation in solar neutrinos.
   - Combining SK, SNO and other experiments, the Large Mixing Angle (LMA) solution is preferred [10]. The oscillation parameters are 2.5×10^{-5} eV^2 $< \Delta m^2 < 3.3 \times 10^{-4}$ eV^2, $0.25 < tan^2\theta < 0.9$ at 3σ bounds.
   - The Kamland [11] observed a rate reduction at the 4.6 σ level of reactor neutrinos($\bar{\nu}_e$) in a flight paths of about 200 km, thus confirming the solar neutrino results of LMA solution.

3. In the above oscillations, there is no indication of the existence of sterile neutrinos at the level of 20% to 30%.

4. $\Delta m^2 \sim 10^{-1}$ eV^2 region

   - The LSND collaboration reported evidence of neutrino oscillation in $\bar{\nu}_\mu \to \bar{\nu}_e$ oscillation in $\Delta m^2 \sim 10^{-1}$ eV^2. However, in a similar experiment, the KARMEN collaboration, with slightly less sensitivity, did not see the effect. If confirmed, to be consistent with LEP experiments, the LSND result would require a fourth kind of neutrino that does not interact with the Z-boson.
   - The Mini-BooNE experiment has started at Fermilab and will either confirm or refute the LSND effect. The results will be available in a few years.

The next-generation experiment should have a high sensitivity/precision to study physics in the lepton sector with a much more powerful and well-controlled neutrino beam, and should proceed beyond 'confirmation' of neutrino oscillation.

1.4 The goal of the first stage of the neutrino experiment at JHF

The first stage of the experiment has three main goals:

1. The discovery of $\nu_\mu \to \nu_e$
   A factor of 20 improvement in sensitivity over the present upper limit is possible in five years running with full operation of the JHF accelerator. The goal is to extend the search down to $\sin^2 2\theta_{13} \simeq 2\sin^2 2\theta_{\mu e} > 0.006$. This measurement is important for two reasons.

   - The mixing angle θ_{13} is the last of the mixing angles in three neutrino scheme. The observation of $\nu_\mu \to \nu_e$ in the first stage of the experiment prove that $\theta_{13} \neq 0$.
   - This is an appearance channel and has a sub-leading oscillation of ν_μ involving Δm^2_{13}. The new developments in solar and reactor neutrino experiments indicate that ν_μ will oscillate to ν_e with a rather large mixing angle and Δm^2_{12}. This oscillation can compete with the one with a mass squared difference of Δm^2_{13}. The former oscillation is suppressed

by a small Δm^2 and the latter is suppressed by the small mixing angle, θ_{13}. Hence, the two processes can compete. This is one of the necessary conditions for a CP violation effect to be observable

2. The precision measurements of oscillation parameters in ν_μ disappearance
   Observation of the oscillation minimum, a 1% measurement (about the same precision as Cabbibo angle in quark sector) of the mixing angle and a 10% measurement of Δm^2 ($\delta(\Delta m^2_{23}) = 10^{-4}$ eV^2 and $\delta(\sin^2 2\theta_{23}) = 0.01$), may show the mixing of second and third generation neutrinos to be consistent with maximal at 1% accuracy. This may impose a constraint on the quark-lepton unification in the future.

3. Search for sterile components in ν_μ disappearance by detecting the neutral-current events
   If a non-zero sterile component is found, the physics of fermions will need modification to accommodate extra member(s) of leptons.

With the successful achievements of the first stage measurements, the construction of 1 Mt Hyper-Kamiokande detector at Kamioka, and a possible upgrade of the accelerator from 0.75 MW to 4 MW in beam power, further experiments can be envisaged. These include another order of magnitude improvement in the $\nu_\mu \to \nu_e$ oscillation sensitivity, a sensitive search for CP violation in the lepton sector (CP phase δ down to $10^\circ - 20^\circ$), and an order of magnitude improvement in proton decay sensitivity.

2 Neutrino beam at JHF

The proton beam is fast-extracted from the 50 GeV PS in a single turn and transported to the production target. The design intensity of the PS is 3.3×10^{14} protons/pulse (ppp) at a repetition rate of 0.285 Hz (3.5 second period), resulting in a beam power of 0.75 MW (2.64 MJ/pulse). The spill width is $\sim$5.2 μsec. We define a typical one-year operation as 10^{21} protons on target (POT), which corresponds to about 130 days of operation. The intensity of the low energy neutrino is almost proportional to the proton beam power (proton energy $\times$ total number of protons per sec.). For the start up period of the accelerator, where a low proton energy and/or a low flux may be expected, the performance of the experiment should be down graded by the available beam power but can nevertheless produce physics results accordingly.

The distance is 295 km between JHF at Tokai and SK at Kamioka. With 295 km baseline, the neutrino energy will be tuned to between 0.4 and 1.0 GeV, which corresponds to Δm^2 between 1.6×10^{-3} and 4×10^{-3} eV^2 suggested by recent SK and K2K results [6] [7].

The layout of JHF facility is drawn in Figure 1. The protons are extracted toward the inside of the PS ring, and are bent by 90° to SK direction by the transport line with a radius of curvature of 107 m. We will adopt superconducting magnets for the transport line. The secondary pions (and kaons) from the target are focused by horns [12], and decay in the decay pipe. The length of the decay pipe from the target position is 130 m. The first front detector is located at 280 m from the target.

We adopt the off axis beam (OAB) configuration. The OAB is the method to produce a narrow neutrino energy spectrum [13]. The axis of the beam optics is displaced by a few degrees from the far detector direction (off-axis). With a finite decay angle, the neutrino energy becomes almost

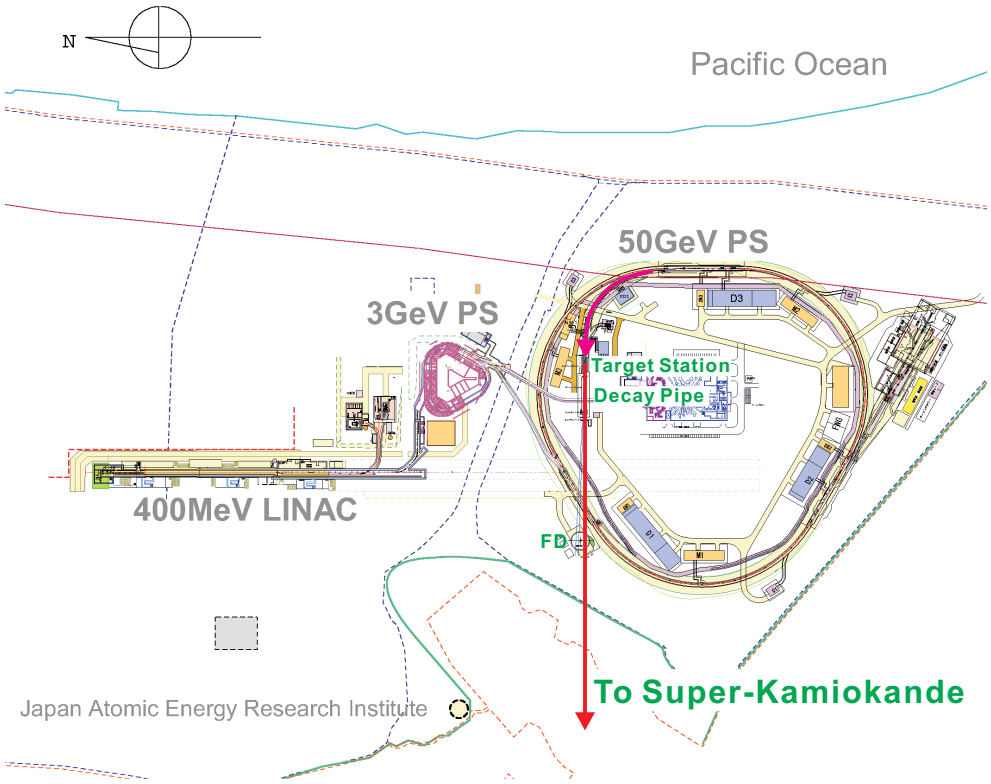

Figure 1: Layout of JHF.

Table 1: Summary of ν_μ beam simulation. The peak energy E_{peak} is in GeV. The flux is given in $10^6/\mathrm{cm}^2/\mathrm{yr}$, and the ν_e/ν_μ flux ratio is in %. The ratio in the "total" column is the one integrated over neutrino energy and the column "E_{peak}" is the ratio at the peak energy of ν_μ spectrum. The normalization for the number of interactions are /22.5kt/yr. The numbers outside (inside) the bracket are number of total (CC) interactions.

		Flux		ν_e/ν_μ(%)		# of interactions	
Beam	E_{peak}	ν_μ	ν_e	total	E_{peak}	ν_μ	ν_e
OA2°	0.7	19.2	0.19	1.00	0.21	3100(2200)	60(45)
OA3°	0.55	10.6	0.13	1.21	0.20	1100(800)	29(22)

independent of parent pion momentum due to characteristics of the Lorenz boost, thus providing the narrow spectrum. The peak neutrino energy can be adjusted by choosing the off-axis angle. ν_μ and $\bar{\nu}_\mu$ can be switched by flipping the polarity of the horn magnets.

Monte-Carlo (MC) simulations using GEANT [14] have been used to estimate the expected neutrino spectra and number of events. The target is assumed to be a simple carbon rod of 1-cm diameter and 1-m long. The Calor-Fluka model [15] is used in the present simulation. From the observed event rate at the near detector of K2K, the beam MC is known to provide absolute neutrino flux with an error better than 20%.

Fig. 2(a) shows expected neutrino energy spectrum of charged current interactions at SK. Fluxes and numbers of interactions are summarized in Table 1. The OAB is roughly a factor of three more intense than possible momentum selected beam. The ν_e contamination in the beam is expected to be 1% at the off-axis angle of 2° (OA2°). The sources of ν_e are $\pi \to \mu \to e$ decay chain and K decay (K_{e3}). Their fractions are μ-decay: 37%, K-decay: 63% for OA2°. The energy spectra of the

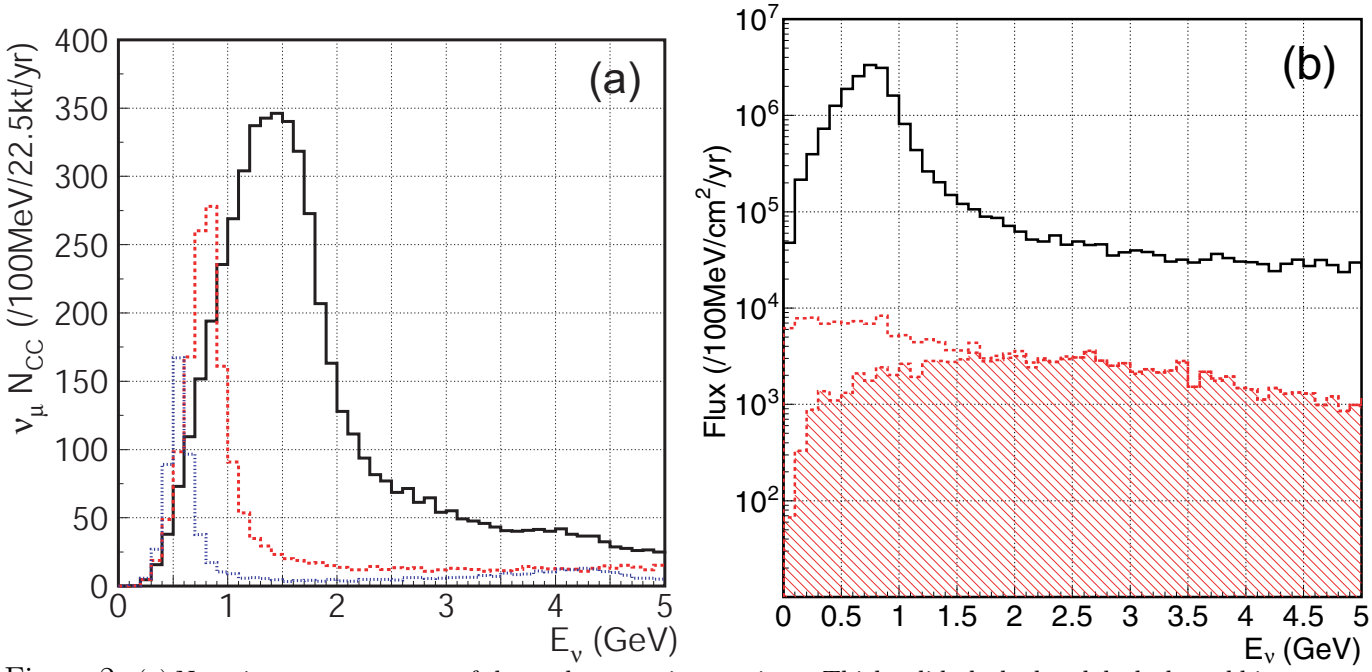

Figure 2: (a) Neutrino energy spectra of charged current interactions. Thick solid, dashed and dash-dotted histograms are OA1°, OA2° and OA3°, respectively. (b) Comparison of ν_e and ν_μ spectra OA2°. Solid (black) histogram is ν_μ and dashed (red) one is ν_e. Hatched area is contribution from K decay. The low energy ν_e component is due to μ decay.

ν_e contamination are plotted in Fig. 2(b). At the peak energy of the ν_μ spectrum, the ν_e/ν_μ ratio is as small as 0.2% in OAB. This indicates that beam ν_e background is greatly suppressed (factor ~ 4) by applying an energy cut on the reconstructed neutrino energy.

Finally, we mention an option of the off-axis beam. One disadvantage of the off-axis beam is relative difficulty in changing the neutrino beam energy after constructing the beam line. The beam line must be re-aligned if one wants to change the beam energy. A relatively easy method to change the neutrino beam energy after finishing the beam line construction is to install a bending magnet after the horns. Detailed Monte Carlo studies have been carried out to study the effect of the bending magnet on the neutrino flux. In the present study, the primary beam line was aligned 2.6° off-axis, and the secondary beam was bent toward or against the far detector by the bending magnet. The Monte Carlo results show that the neutrino flux by this scheme and the conventional off-axis scheme is almost identical for off-axis angles between 2 and 3 degrees. Therefore, we are seriously considering this scheme as a possible beam line option, and various engineering studies are in progress.

3 Near detectors

3.1 Muon monitor

The direction of the proton beam is monitored by the muon monitor, which measures high energy muons passing through the beam dump. The detector is located in the muon pit that is located down stream of the beam dump. The proton beam direction can be monitored with an accuracy of better than 1 mrad for each spill by segmented ionization chamber and/or semi-conductor detector. The muon monitor also tracks the stability of the neutrino yield.

3.2 Near detector at 280 m from the target

The near detector hall will be located at 280 m from the target as shown in Figure 1. The diameter is 20 m and the depth is 40 m to cover the off-axis angle between 0° to 3°. The role of the near detectors is to provide predictions of the expected neutrino at the far detector. The near detector is required to have a capability of identifying both event type (CCQE, ν_μ and ν_e inelastic events, neutral current events) and should be able to measure the neutrino spectrum at the near location. A fully-active fine-grained scintillator tracker, similar to the one for the K2K upgrade [16], is considered as a candidate for the near detector at 280 m. With sufficient granularity, the detector can fully reconstruct quasi-elastic scattering events ($\nu_\mu n \to \mu^- p$) by tagging recoil protons, and identify pions from inelastic scatterings. The detector should have enough radiation length to measure the energies and directions of electrons from the ν_e interaction and π^0's from the neutral current reactions.

In an ideal case, all the systematic uncertainty would cancel out by using the measured spectra in the near detector. In reality, the near detectors are different from the far detector in terms of material, size (radiation length), and responses. The closer location to the decay pipe also introduces a large and complicated far-to-near spectrum ratio. In Figure 3, spectra at the far and near sites are compared. The peak postion is shifted to higher energy at the far site than at the near site. The far/near spectrum ratio is also plotted in the figure. The difference is as large as 40∼50%. The

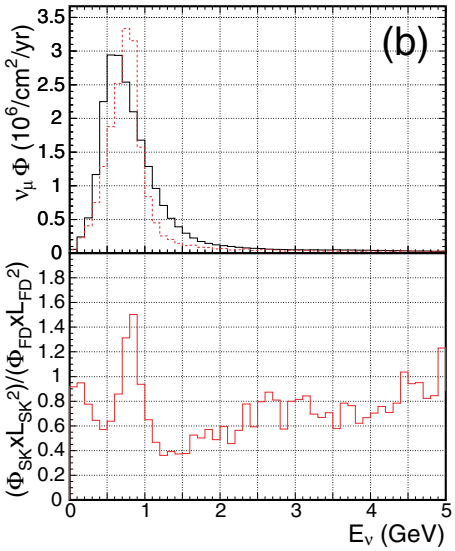

Figure 3: Comparison of spectra at far and near site for OA2°. Upper figure is ν_μ spectra at 280 m (solid black histogram) and 295 km (dashed red histogram). The flux for the near site is multiplied by $(295/0.28)^2$ to directly compare the spectra. The near detector size is assumed to be ±5 m in horizontal and vertical directions. The lower plots are far/near ratio of fluxes.

sources of this far/near difference are the difference in the solid angle between far and near detectors and the finite length of decay pipe; the neutrino source is point like for the far detector, but the length of the decay pipe is not negligible for the near detector. At distances longer than one km or more from the target, both of the above two effects become negligible and the far/near ratio becomes flat.

One solution to this challenge is to place a detector similar to the far detector further away from the production target. This will be discussed in the next section. Another approach, which can be taken for the 280 m detector, is to understand the beam and the detector responses in detail and correct for the differences. Ultimately, systematic uncertainties will be estimated by comparing both of these two approaches.

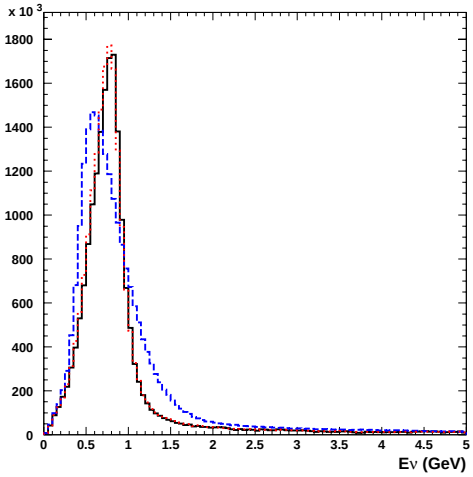

Figure 4: Calculated energy spectrum of the neutrino flux at Super-Kamiokande (solid) and at 280 m (dashed) and 1.5 km (dotted) distances from the neutrino production target for the 2° off-axis beam. The vertical axis is arbitrary.

The challenge in understanding the neutrino beam is that only the "product" of neutrino flux, neutrino cross section, and detection efficiency is observable. The flux can be measured by quasi-elastic scattering events, which have a clean signature and a reliable cross section estimate. Cross sections as a function of the neutrino energy can be measured by placing the near detector at different off-axis locations providing different ν_μ peak energies. Since the scintillator is composed of carbon, scintillator that contains oxygen (or water) could be considered to measure the cross section difference between carbon and oxygen.

Finally, the stability of the beam direction and the flux will be monitored by detecting neutrinos in the 0° direction. This measurement complements the measurements by the proton beam monitor and the muon monitor in the beam dump.

4 Intermediate detector

In order to achieve the final designed goals of the experiment, it is important to measure the neutrino beam at an intermediate position, where the neutrino spectra are similar to those at Super-Kamiokande, so that various detector systematics cancel by taking the far-near ratio.

We propose to construct a water Cherenkov detector at intermediate position to cancel detector systematics as much as possible. Figure 4 compares the calculated energy spectrum at Super-Kamiokande and at 280 m and 1.5 km distances from the neutrino production target for the 2° off-axis beam. 280 m is the near on-site neutrino detector position. The spectrum has a lower energy peak at 280 m, as mentioned before, while the 1.5 km and Super-Kamiokande spectra are almost identical. According to the beam Monte Carlo, the "far-near" ratio ($\equiv$ flux(far)/flux(near)$\times(L_{far}/L_{near})^2$) approaches unity very quickly as L_{near} increases, where L_{far} (L_{near}) is the distance between the production target and the far (near) detector. For L_{near} >1.0 km, the deviation from unity is less than 10%.

The most demanding goal for the precision of the systematic error is the background subtraction

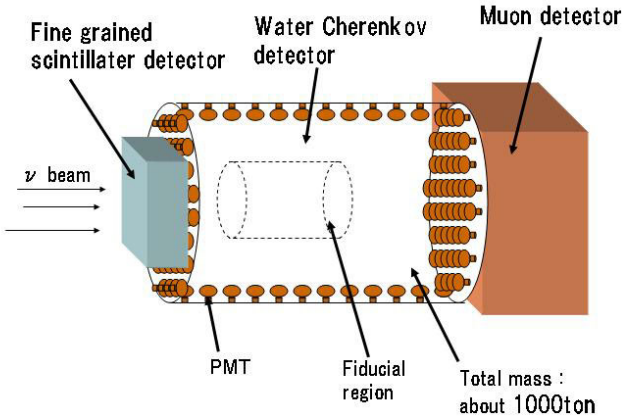

Figure 5: A possible design of the intermediate detector to be installed at about 2 km from the target.

for the $\nu_\mu \to \nu_e$ search and a CP violation search (see Figure 10). A 2% subtraction error is our goal, which is possible for 10% corrections due to the spectrum difference at the intermediate and the far detector.

From event rate considerations, we estimate that the fiducial mass of the intermediate detector should be about 100 tons, assuming that the detector is installed 2 km from the target. We also require that the distance from the surface of the fiducial volume to the PMTs is 2 m following the definition in Super-Kamiokande. In addition, this detector has to measure the energy of muons up to about 1 GeV. For this reason, the distance from the surface of the fiducial volume to the PMTs should be about 4 m for the down-stream region. The fiducial volume can be 4 m in diameter and 8 m in length, and the total volume (including the volume for installing PMTs) can be about 9 m in diameter and 15 m in length. The total weight is about 1000 tons.

In addition to the water Cherenkov detector, it is important to install muon range counters down stream to measure the energies of high energy muons that are produced by the high energy tail of the flux. Furthermore, a fine-grained scintillator detector should be installed in front of the water Cherenkov detector in order to study the details of neutrino interaction kinematics. Figure 5 shows a possible design of the intermediate detector to be installed approximately 2 km from the target.

5 Far detector: Super-Kamiokande

The far detector, Super-Kamiokande, is located in the Kamioka Observatory, Institute for Cosmic Ray Research (ICRR), University of Tokyo, which has been successfully taking data since 1996. The detector is also used as a far detector for the K2K experiment.

The detector will be fully recovered from the accident in 2001 by the time JHFnu start in 2007. It is a 50,000 ton water Čerenkov detector located at a depth of 2,700 meters water equivalent in the Kamioka mine in Japan. Its performance and results in atmospheric neutrinos and solar neutrinos have been well-documented elsewhere[6, 8, 10].

A schematic view of detector is shown as Fig 6. The detector cavity is 42 m in height and 39 m in

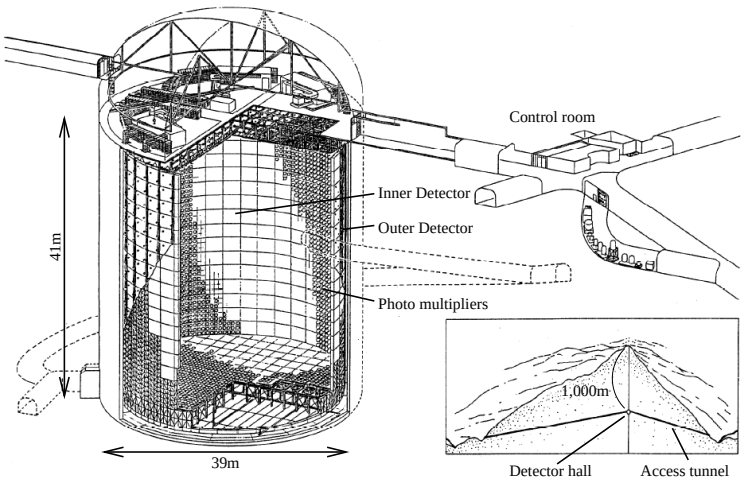

Figure 6: A schematic view of the Super-Kamiokande Detector.

diameter, filled with 50,000 tons of pure water. There is an inner detector (ID), 33.8 m diameter and 36.2 m high, surrounded by an outer detector (OD) approximately 2 m thick. The inner detector has 11,146, 50 cm ϕ PMTs, instrumented on a 70.7 cm grid spacing on all surface of the inner detector. The outer detector is instrumented with 1,885, 20 cm ϕ PMTs and is used as an anti-counter to identify entering/exiting particles to/from ID. The fiducial volume is defined as 2 m away from the ID wall, and the total fiducial mass is 22,500 ton.

The ID PMT's detects Čerenkov rings produced by relativistic charged particles. The trigger threshold was achieved to be 4.3 MeV. The pulse-height and timing information of the PMT's are fitted to reconstruct the vertex, direction, energy, and particle identification of the Čerenkov rings. A typical vertex, angular and energy resolution for a 1 GeV μ is 30 cm, 3° and 3%, respectively. The Čerenkov ring shape, clear ring for muons and fuzzy ring for electrons, provides good e/μ identification. A typical rejection factor to separate μ's from e's (or vice versa) is about 100 for single Čerenkov ring events at 1 GeV. The e's and μ's are further separated by detecting decay electrons from the μ decays. A typical detection efficiency of decay electrons from cosmic stopping muons is roughly 80%, and can be improved by further analysis. A 4π coverage around the interaction vertex provides an efficient π^0 detection and e/π^0 separation as discussed in section 6.2.

Interactions of neutrinos from the accelerator are identified by synchronizing the timing between the beam extraction time at the accelerator and the trigger time at Super-Kamiokande using the Global Positioning System (GPS). The synchronization accuracy of the two sites is demonstrated to be less than 200 ns in the K2K experiment. Because of this stringent time constraint, and the quiet environment of the deep Kamioka mine, chance coincidence of any entering background is negligibly low. A typical chance coincidence rate of atmospheric neutrino events is 10^{-10}/spill, which is much smaller than the signal rate of about $\times 10^{-3}$/spill.

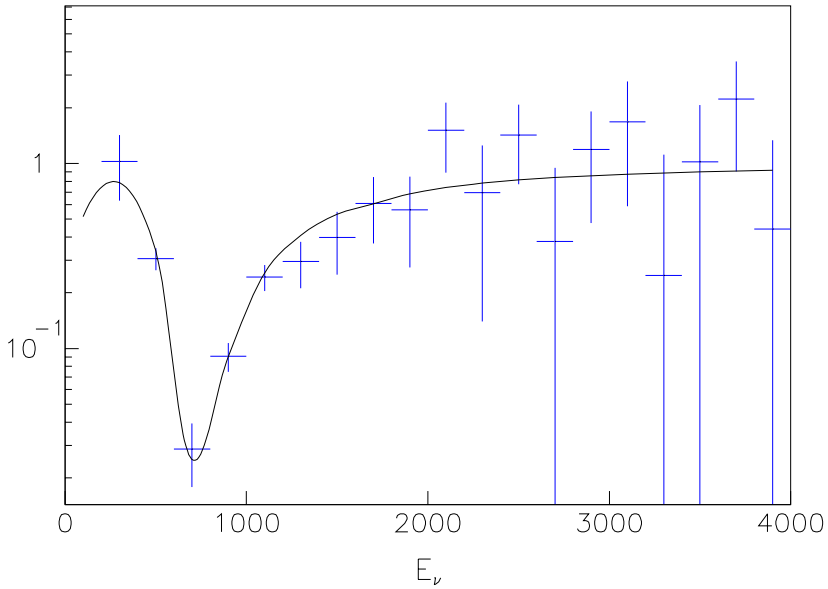

Figure 7: The ratio of the measured spectrum with neutrino oscillation to the expected one without neutrino oscillation after subtracting the contribution of non QE-events. The fit result of the oscillation is overlaid.

6 Physics in the first stage of the project

6.1 High precision measurement of Δm^2_{23} and θ_{23} with ν_μ disappearance

The neutrino energy can be reconstructed through quasi-elastic (QE) interactions (Equation 1) by the Super-Kamiokande (SK) detector. In this analysis, we use the same muon selection criteria as those used in the atmospheric neutrino analysis by the Super Kamiokande collaboration [6]; fully contained single ring muon-like events in a fiducial volume of 22.5 kt.

In this analysis, the exposure time is assumed to be five years and θ_{13} is approximated to be zero. In the oscillation analysis, the neutrino energy spectrum is extracted by subtracting the contribution of non-QE background events. To examine the expected precision of the oscillation parameters determination, full Super-Kamiokande Monte Carlo events are generated. The ratio between the "measured" spectrum at SK and the expected one without oscillation, after subtracting the non-QE contribution, is fitted by the function of $P(\nu_\mu \to \nu_\mu)$:

$$P(\nu_\mu \to \nu_\mu) = 1 - \sin^2 2\theta_{23} \cdot \cos^4 \theta_{13} \cdot \sin^2(1.27\Delta m^2_{23}[eV^2]L[km]/E_\nu[GeV]) \quad (2)$$

Since the spectrum of non-QE events depends on the oscillation parameters, the non-QE spectrum is updated by the fit result at each iteration of the fitting. The survival probability of $P(\nu_\mu \to \nu_\mu)$ is shown in Figure 7, which gives the fit result of $(\Delta m^2_{23}, \sin^2 2\theta_{23}) = ((2.96 \pm 0.04) \times 10^{-3}\mathrm{eV}^2, 1.0 \pm 0.01)$. The oscillation pattern is clearly seen and a $\sin^2 2\theta_{23}$ precision of 1 % and a Δm^2_{23} precision of 4×10^{-5} eV^2 are expected.

Several beam configurations are studied in the range of Δm^2_{23} between 1×10^{-3} and 1×10^{-2} eV^2. The result is summarized in Figure 8. With OA2°, the maximum sensitivity to the oscillation parameters is achieved at $\Delta m^2_{23} = (3 \sim 3.5) \times 10^{-3}$ eV^2. In the case of $\sin^2 2\theta_{23} = 0.9$, which is the lower bound suggested by atmospheric neutrino result of Super-Kamiokande, the precision is slightly worse due to non-oscillated neutrino events at the oscillation maximum.

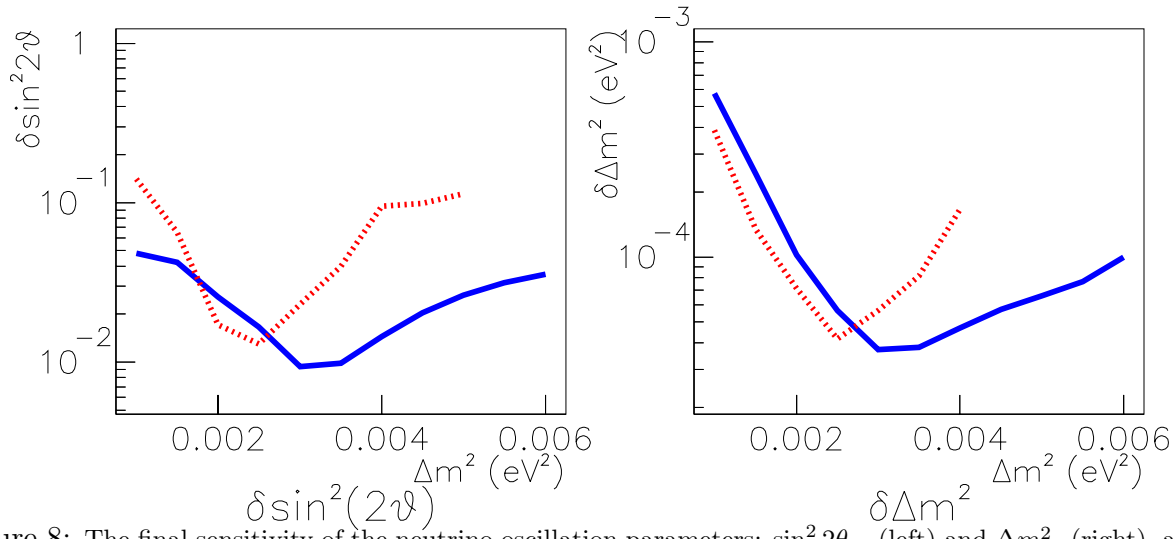

Figure 8: The final sensitivity of the neutrino oscillation parameters: $\sin^2 2\theta_{23}$ (left) and Δm^2_{23} (right), as a function of true Δm^2_{23} (eV^2). The $\sin^2 2\theta_{23}$ is set to 1.00. The result with OA2° is shown by the blue (solid) line, OA3° by the red (dashed) line.

By selecting the bin at the oscillation maximum, the disappearance signal dip is enhanced and thus the contribution of the systematic uncertainties are largely suppressed. For example, the depth of the dip in Figure 7, which corresponds to $1 - \sin^2 2\theta_{23}$, is as small as 3%. Thus, a systematic uncertainty of 10% in the flux normalization (far/near ratio) contributes to 3% $\times$ 0.1 =0.3% in the $\sin^2 2\theta_{23}$ measurement. Assuming 10% systematic uncertainty in the far/near ratio, which is similar to K2K's number of 6%, 4% uncertainty in the energy scale, and 20% uncertainty in the non-QE background subtraction, the total systematic error is estimated to be less than 1 % for $\sin^2 2\theta_{23}$ and less than 1×10^{-4} eV^2 for Δm^2_{23}.

The systematic uncertainties are expected to be reduced further below the statistical uncertainties by the neutrino flux measurement using QE events and detailed non-QE background measurement by the front detector, by the pion production measurement, and possibly by an intermediate detector at a few km point which makes the systematics in the far/near ratio negligible.

The overall sensitivity is expected to be 1% in precision for $\sin^2 2\theta_{23}$ and better than 1×10^{-4} eV^2 for Δm^2_{23}.

6.2 ν_e appearance search

The JHF neutrino beam has small ν_e contamination (0.2% at the peak energy of OAB) and the ν_e appearance signal is enhanced by tuning the neutrino energy at its expected oscillation maximum. Thus, JHFnu experiment has an excellent opportunity to discover ν_e appearance and thus measure θ_{13}. The sensitivity on ν_e appearance is described based on the full Monte Carlo simulations and analysis of Super-Kamiokande and K2K experiments.

The process of the ν_e appearance signal is searched for in the CCQE interaction, for which the energy of neutrino can be calculated to take advantage of the narrow band neutrino beam. Since the proton momentum from the QE interaction is usually below the Čerenkov threshold, the signal has only a single electro-magnetic shower (single ring e-like).

Table 2: Number of events and reduction efficiency of "standard" 1ring e-like cut and π^0 cut for 5 year exposure (5×10^{21} p.o.t.) OA2°. For the calculation of oscillated ν_e,$\Delta m^2 = 3 \times 10^{-3}$ eV^2 and $\sin^2 2\theta_{\mu e} = 0.05$ is assumed.

OAB 2°	ν_μ C.C.	ν_μ N.C.	Beam ν_e	Oscillated ν_e
1) Generated in F.V.	10713.6	4080.3	292.1	301.6
2) 1R e-like	14.3	247.1	68.4	203.7
3) e/π^0 separation	3.5	23.0	21.9	152.2
4) 0.4 GeV< E_{rec} < 1.2 GeV	1.8	9.3	11.1	123.2

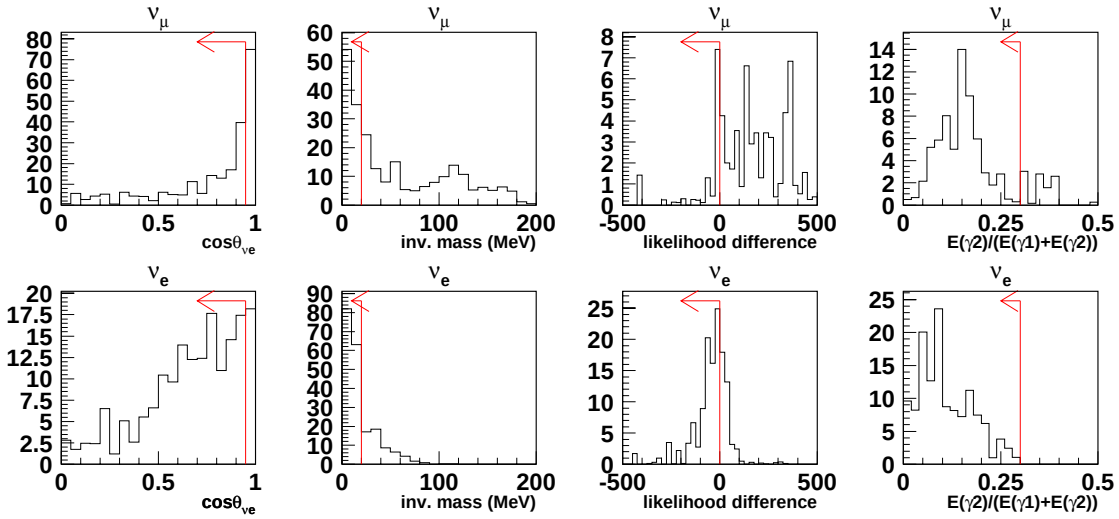

Figure 9: Distributions of the quantities, used in the e/π^0 separation. The beam is the off-axis 2 degree beam and events are after the single-ring e-like selection. Upper histograms corresponds to ν_μ background events and the lower histograms correspond to the ν_e signal events. The arrows in the figure show the cut positions used in the analysis.

The standard Super-Kamiokande atmospheric neutrino analysis criteria are used to select single ring e-like events: single ring, electron like (showering), visible energy greater than 100 MeV, and no decay electrons. Reduction of number of events by the "standard" 1 ring e-like cut for charged and neutral current events are listed in Table 2. The excellent e/μ separation capability and $\mu \to e$ detecting capability are key features of the effective elimination of ν_μ charged current and all of the inelastic events which contain charged π. The remaining background events at this stage are predominantly from single π^0 production through neutral current interactions and from ν_e contamination in the beam.

Figure 9 shows distributions of four characteristic quantities that separates signal ν_e events from π^0 background events, as follows:

1. Angle between ν and e ($\cos\theta_{\nu e}$):
   Some fraction of π^0 background has a steep forward peak, which is likely due to coherent π^0 production. Those events in the extreme forward direction are rejected.

2. Invariant mass of 2 photons:
   The π^0 background shows a peak at 135 MeV whereas the ν_e signal shows small invariant mass. Those events with large invariant mass are rejected.

3. Difference between double and single ring likelihoods:

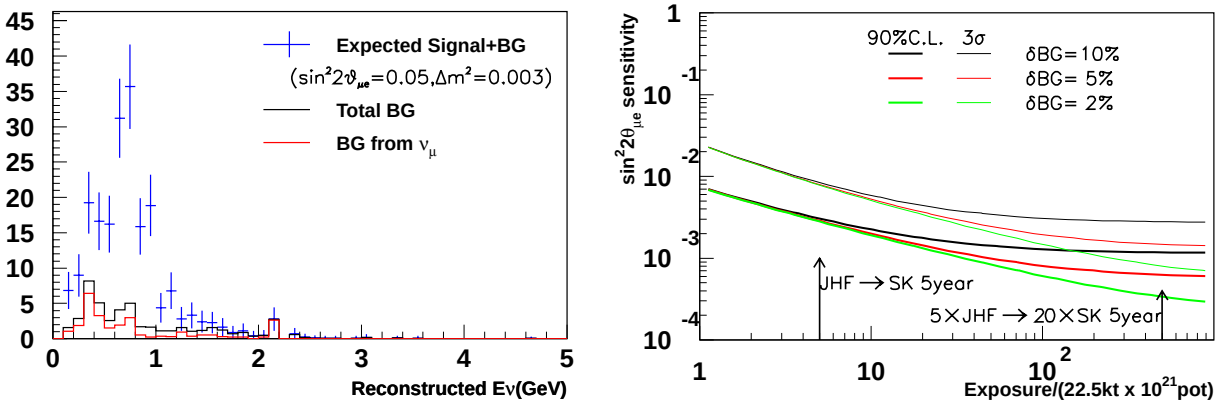

Figure 10: Left:Expected reconstructed neutrino energy distributions of expected signal+BG, total BG, and BG from ν_μ interactions for 5 years exposure of OA2°. Right: Expected (thick lines:) 90%CL sensitivity and (thin lines:) 3σ discovery contours as the functions of exposure time of OA2°. In left figure, expected oscillation signals are calculated with the oscillation parameters: $\Delta m^2 = 3 \times 10^{-3}$ eV^2,$\sin^2 2\theta_{\mu e}(effective mixing angle = \sin^2\theta_{23} \cdot \sin^2 2\theta_{13}) = 0.05$.(see Appendix) In the right figures, three different contours correspond to 10%, 5%, and 2% uncertainty in the background estimation.

For neutrino energies below 1 GeV, the main limitation to separate electrons from π^0s comes from asymmetric decay of π^0s, where the lower energy photon tends to be hidden under the scattered light of the higher energy photon. In order to further suppress the π^0 background, the PMTs hit pattern including scattered light is fitted and two likelihoods are calculated; one assuming that the event contains one ring and the other assuming two showing rings. Single ring like events are selected based on the difference of the two likelihoods.

4. Energy fraction of lower energy ring ($\frac{E(\gamma_2)}{E(\gamma_1)+E(\gamma_2)}$)
The ν_e signal tends to have a low energy second ring which is either a fake ring or a ring due to bremsstrahlung. Those events with the large energy fraction are rejected.

Table 2 lists the number of events after this e/π^0 separation. An order of magnitude extra rejection (23/247.1) in the ν_μ neutral current background is achieved with 152.2/203.7=75% in signal acceptance.

Figure 10 (left) shows the reconstructed neutrino energy distributions for 5 years. The oscillation parameters of $\Delta m^2 = 3 \times 10^{-3}$ eV^2 and $\sin^2 2\theta_{13} = 0.1$ are assumed. A clear appearance peak is seen at the oscillation maximum of E_ν ~0.75 GeV. The right plot of Figure 10 show 90% and 3σ limits as a function of the years of operation with the systematic uncertainty of background subtraction to be 2%, 5% and 10%. The sensitivity of $\sin^2 2\theta_{13} = 0.006$ at 90% confidence level can be achieved in five years of operation. Figure 11 shows 90%C.L. contours for 5 year exposure of each beam configuration assuming 10% systematic uncertainty in background subtraction.

6.3 Search for sterile neutrinos (ν_s) in ν_μ disappearance

Neutral current (NC) events represent the sum of $\nu_\mu \to \nu_e, \nu_\mu$, and ν_τ oscillations. Therefore, NC measurement combined with $\nu_\mu \to \nu_e$ and $\nu_\mu \to \nu_\mu$ measurements provide indirect measurement of the $\nu_\mu \to \nu_\tau$ and $\nu_\mu \to \nu_s$ oscillation.

In the JHF sub-GeV neutrino beam, the dominant detectable NC interactions are single π productions. Among those, single π^0 production process is selected to study NC events, because of a unique signature. The following selection criteria are used to select NC π^0 events.

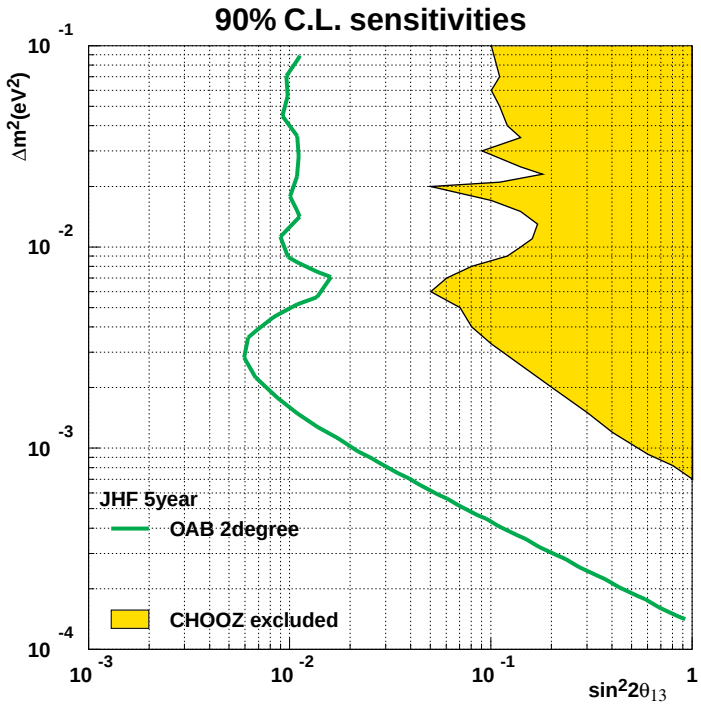

Figure 11: The 90% C.L. sensitivity contours in 5 years of operation with OA2°. The 90% C.L. excluded region of CHOOZ is plotted as a comparison. $sin^2\theta_{23}$ is assumed to be 0.5 and the possible contribution due to θ_{12} term is assumed to be small compared to the one due to θ_{13} term.

1. The event must be fully contained,
   The total energy deposit in the detector (E_{vis}) is used to reject high energy events. E_{vis} is required to be greater than 100 MeV and less than 1500 MeV.

2. The number of Cherenkov rings in an event must be less than three and they must be electron-like to eliminate background from CC inelastic interactions with a π^0.

3. To further eliminate CC events, no decay electron is required. In the Super-Kamiokande analysis, the efficiency of detecting the decay electrons is 80%.

The expected numbers of events as a function of Δm^2 are shown in Figure 12. In the figures, maximal oscillations, $\sin^2 2\theta$=1.0, is assumed. The dotted lines in each figure correspond to the 90% C.L. limit for $\nu_\mu \rightarrow \nu_\tau$ oscillations assuming a systematic uncertainty of 5%. The expected numbers of events for $\nu_\mu \rightarrow \nu_\tau$ and for $\nu_\mu \rightarrow \nu_s$ are clearly separated if the Δm^2 is larger than 1×10^{-3} for OAB.

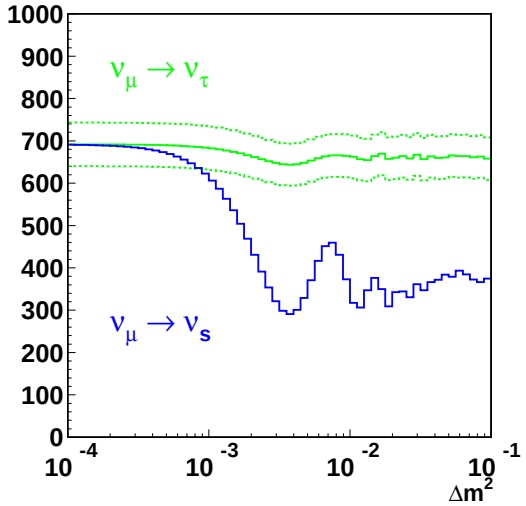

Figure 12: Expected number of events with various Δm^2 for 5 years of OA2°. The solid lines show the expected numbers of events assuming $\nu_\mu \rightarrow \nu_\tau$ or $\nu_\mu \rightarrow \nu_s$. The dotted lines show the 90% C.L. regions of $\nu_\mu \rightarrow \nu_\tau$ oscillation. Although full mixing is assumed, expected number of events does not become 0 even at the deepest dip point. This is due to the NC interactions of high energy neutrinos. For $\Delta m^2 = 3 \times 10^{-3} eV^2$, the number of events to be observed in five years is 280, if $\nu_\mu \rightarrow \nu_s$. The corresponding number is 680 for $\nu_\mu \rightarrow \nu_\tau$oscillation.

Appendix

A Neutrino oscillation

Lepton mixing is described by a unitary 3x3 matrix (Maki-Nakagawa-Sakata [4] (MNS) matrix) that is defined by a product of three rotation matrices with three angles (θ_{12}, θ_{23}, and θ_{13}) and a complex phase (δ) as in the Cabibbo-Kobayashi-Maskawa matrix [5].

$$\begin{pmatrix} \nu_e \\ \nu_\mu \\ \nu_\tau \end{pmatrix} = \begin{bmatrix} U_{\alpha i} \end{bmatrix} \begin{pmatrix} \nu_1 \\ \nu_2 \\ \nu_3 \end{pmatrix}, \tag{3}$$

$$U = \begin{pmatrix} 1 & 0 & 0 \\ 0 & C_{23} & S_{23} \\ 0 & -S_{23} & C_{23} \end{pmatrix} \begin{pmatrix} C_{13} & 0 & S_{13}e^{-i\delta} \\ 0 & 1 & 0 \\ -S_{13}e^{i\delta} & 0 & C_{13} \end{pmatrix} \begin{pmatrix} C_{12} & S_{12} & 0 \\ -S_{12} & C_{12} & 0 \\ 0 & 0 & 1 \end{pmatrix}, \tag{4}$$

where $\alpha = e,\ \mu,\ \tau$ are the flavor indices, i=1, 2, 3 are the indices of the mass eigenstates, S_{ij} (C_{ij}) stands for $\sin\theta_{ij}$ ($\cos\theta_{ij}$). Neutrinos are produced as flavor eigenstates and each component of mass eigenstate gets a different phase after traveling a certain distance. The detection of neutrinos by charged current interactions projects these new states back onto flavor eigenstates. The probability of oscillation is given by the formula,

$$\begin{aligned} P(\nu_\alpha \rightarrow \nu_\beta) = \delta_{\alpha\beta} \quad &- \quad 4\sum_{i>j} Re(U^*_{\alpha i}U_{\beta i}U_{\alpha j}U^*_{\beta j}) \cdot \sin^2\Phi_{ij} \\ &\pm \quad 2\sum_{i>j} Im(U^*_{\alpha i}U_{\beta i}U_{\alpha j}U^*_{\beta j}) \cdot \sin 2\Phi_{ij} \end{aligned} \tag{5}$$

where

$$\Phi_{ij} \equiv \Delta m^2_{ij} L/4E_\nu = 1.27\Delta m^2_{ij}[eV^2]L[km]/E_\nu[GeV], \tag{6}$$

$\Delta m^2_{ij} = m^2_j - m^2_i$, L is the flight distance, and E_ν is the neutrino energy. The $\pm$ sign in the third term is the CP violation effect, $-$ for neutrinos and $+$ for anti-neutrinos. Because $\Delta m^2_{12} + \Delta m^2_{23} + \Delta m^2_{31} = 0$, there exist only two independent Δm^2 for three species of neutrinos. Thus 3 generation neutrino oscillation can be described by two Δm^2's, three angles $(\theta_{12}, \theta_{23}, \theta_{13})$ and one phase (δ).

We take the two Δm^2 values as the values suggested by solar and atmospheric neutrino measurements (including the recent Kamland results); $\Delta m^2_{12} = \Delta m^2_{sol} \simeq (6 \sim 9) \times 10^{-5}$ or $(1.3 \sim 2.0) \times 10^{-4} eV^2$ and $\Delta m^2_{23} \simeq \Delta m^2_{31} \equiv \Delta m^2_{atm} = (1.6 \sim 4) \times 10^{-3}$ eV^2.

For an oscillation measurement with $E_\nu \simeq \Delta m^2_{23} \cdot L$ as in this proposed experiment, the contribution of Δm^2_{12} term is small and the oscillation probabilities can be approximately expressed by two mixing angles;

$$
\begin{aligned}
P(\nu_\mu \to \nu_e) &= \sin^2 2\theta_{13} \cdot \sin^2 \theta_{23} \cdot \sin^2 \Phi_{23}, && (7)\\
P(\nu_\mu \to \nu_\mu) &= 1 - \sin^2 2\theta_{23} \cdot \cos^4 \theta_{13} \cdot \sin^2 \Phi_{23} - P(\nu_\mu \to \nu_e), && (8)\\
P(\nu_e \to \nu_\tau) &= \sin^2 2\theta_{13} \cdot \cos^2 \theta_{23} \cdot \sin^2 \Phi_{23}, && (9)\\
P(\nu_e \to \nu_e) &= 1 - \sin^2 2\theta_{13} \quad \cdot \quad \sin^2 \Phi_{23}. && (10)
\end{aligned}
$$

If we define effective mixing angles as $\sin^2 2\theta_{\mu e} \equiv \sin^2 2\theta_{13} \cdot \sin^2 \theta_{23}$ and $\sin^2 2\theta_{\mu\tau} \equiv \sin^2 2\theta_{23} \cdot \cos^4 \theta_{13}$, then the expressions reduce to the ones in the two flavor approximation;

$$
\begin{aligned}
P(\nu_\mu \to \nu_e) &= \sin^2 2\theta_{\mu e} \cdot sin^2 \Phi_{23}, && (11)\\
P(\nu_\mu \to \nu_\mu) &= 1 - \sin^2 2\theta_{\mu\tau} \cdot sin^2 \Phi_{23} - P(\nu_\mu \to \nu_e). && (12)
\end{aligned}
$$

Experimental constraints obtained from ν_μ disappearance in the atmospheric neutrino measurements are $\sin^2 2\theta_{\mu\tau} > 0.89$ and $1.6 \times 10^{-3} < \Delta m^2_{23} < 4 \times 10^{-3}$ eV^2 [6]. Solar neutrino and Kamland results allow the large mixing angle solution, LMA: $\Delta m^2_{12} = \simeq (6 \sim 9) \times 10^{-5}$ or $(1.3 \sim 2.0) \times 10^{-4} eV^2$ and $0.73 < \sin^2 2\theta_{12} < 0.97$ at 95% C.L. [9, 10, 11]. The most stringent constraint on θ_{13} comes from reactor $\bar{\nu}_e$ disappearance experiments. As can be seen in eq. (10), $\bar{\nu}_e$ disappearance directly measures θ_{13}. The current limit is $\sin^2 2\theta_{13} < 0.05$ for $\Delta m^2_{23} \simeq 6 \times 10^{-3}$ eV^2 and $\sin^2 2\theta_{13} \leq 0.12$ for $\Delta m^2_{23} \simeq 3 \times 10^{-3}$ eV^2 at 90 % C.L [17]. Since θ_{13} is very small and atmospheric neutrino data indicates almost full mixing $\theta_{23} \simeq \pi/4$, the effective two flavor mixing angles defined above and 3 flavor angles have the following approximate relations;

$$
\sin^2 2\theta_{\mu\tau} \simeq \sin^2 2\theta_{23}, \qquad \sin^2 2\theta_{\mu e} \simeq \frac{1}{2} \sin^2 2\theta_{13} \simeq 2 \left| U_{e3} \right|^2 . \tag{13}
$$

It follows from eq. (5) that CP violation can be observed only with appearance experiments, since $Im(U^*_{\alpha i} U_{\beta i} U_{\alpha j} U^*_{\beta j}) = 0$ for $\alpha = \beta$. Especially $\nu_\mu \leftrightarrow \nu_e$ oscillation is known to provide the best chance of measuring CP asymmetry in the lepton sector. This is because the leading CP conserving term of $\nu_\mu \leftrightarrow \nu_e$ oscillation is highly suppressed due to small Δm^2_{12} and the subleading terms, such as U_{e3} related and CP violating terms, give leading contributions, as shown below. If the oscillation $\nu_\mu \to \nu_e$ is at the observable level in the first phase of the project, further investigation of CP violation will be carried out in the second phase. In addition, since CP violation in three generations requires that all three members should be involved in the process, solar neutrino related quantities (θ_{12}, Δ_{12}) must be large (namely the large mixing angle solution for solar neutrino oscillation) in order for CP violation in neutrino oscillations to be observable.

The $\nu_\mu \to \nu_e$ appearance probability can be written using MNS matrix element as [18]

$$\begin{aligned} P(\nu_\mu \to \nu_e) = & \quad 4C_{13}^2 S_{13}^2 S_{23}^2 \sin^2\Phi_{31} \\ & + \; 8C_{13}^2 S_{12} S_{13} S_{23} (C_{12} C_{23} \cos\delta - S_{12} S_{13} S_{23}) \cos\Phi_{32} \cdot \sin\Phi_{31} \cdot \sin\Phi_{21} \\ & - \quad 8C_{13}^2 C_{12} C_{23} S_{12} S_{13} S_{23} \sin\delta \sin\Phi_{32} \cdot \sin\Phi_{31} \cdot \sin\Phi_{21} \\ & + \; 4S_{12}^2 C_{13}^2 \left(C_{12}^2 C_{23}^2 + S_{12}^2 S_{23}^2 S_{13}^2 - 2C_{12} C_{23} S_{12} S_{23} S_{13} \cos\delta\right) \sin^2\Phi_{21} \\ & - \quad 8C_{13}^2 S_{13}^2 S_{23}^2 \left(1 - 2S_{13}^2\right) \frac{aL}{4E_\nu} \cos\Phi_{32} \sin\Phi_{31}. \end{aligned} \tag{14}$$

The first term has the largest contribution. The second cosδ term is generated by the CP phase δ but is CP conserving. The third sinδ term violates CP. The fourth term, which is the solar neutrino term, is suppressed by $\sin^2 \frac{\Delta m_{21}^2 L}{4E_\nu}$. The matter effect is characterized by

$$a = 2\sqrt{2} G_F n_e E_\nu = 7.6 \times 10^{-5} \rho[g/cm^3] E_\nu[GeV] \qquad [eV^2], \tag{15}$$

where G_F is the Fermi constant, n_e is the electron density and ρ is the earth density. The probability $P(\bar{\nu}_\mu \to \bar{\nu}_e)$ is obtained by the replacing $a \to -a$ and $\delta \to -\delta$ in eq. (14). As seen in eq. (15) the matter effect is proportional to neutrino energy, so the lower the energy, the smaller the effect is. The CP asymmetry in the absence of the matter effect is calculated as

$$A_{CP} \;=\; \frac{P(\nu_\mu \to \nu_e) - P(\bar{\nu}_\mu \to \bar{\nu}_e)}{P(\nu_\mu \to \nu_e) + P(\bar{\nu}_\mu \to \bar{\nu}_e)} \simeq \frac{\Delta m_{12}^2 L}{4E_\nu} \cdot \frac{\sin 2\theta_{12}}{\sin\theta_{13}} \cdot \sin\delta \tag{16}$$

Because θ_{13} is small, the CP asymmetry can be large, especially for small E_ν.

B Physics in the future extension with Hyper-Kamiokande

In the 2nd phase of the JHF-Kamioka neutrino experiment, the proton intensity is planned to go up to 4 MW [19]. The pion (or neutrino) production target will also be upgraded to a liquid metal target to accept the 4 MW beam. The shielding of the decay pipe will be designed to accommodate such a beam.

As for the far detector, Hyper-Kamiokande detector is proposed as a next generation large water Čerenkov detector [20] at Tochibora zinc mine in Kamioka, which is about 8 km south of the Super-Kamiokande detector. A schematic view of one candidate detector design is shown in Figure 13. A 500 m long water tank is made from 10 sub-detectors, each one 50 m long. The tank will be filled with pure water, and photomultiplier tubes (PMTs) are instrumented on all surfaces of sub-detectors. The fiducial volume of the detector is about 0.54 Mt. The outer detectors, with thicknesses of at least 2.0 m, completely surround the inner sub-detectors, and the outer region is also instrumented with PMTs. The primary function of the outer detectors is to veto cosmic ray muons and to help identify contained events. The Kamioka site satisfies the conditions required for constructing large water Čerenkov detectors: easy access to underground, clean water, hard and uniform rock, and infrastructure/technology for excavation. The overburden of the Hyper-Kamiokande is expected to be about 1500 meter-water-equivalent.

With these upgrades in both accelerator (×5) and detector (×25), the statistics is expected to increase by more than a factor of 100. The goal of the second phase is

- $\sin^2 2\theta_{13}$ sensitivity below 10^{-3}
- CP phase δ measurement down to 10-20 degrees

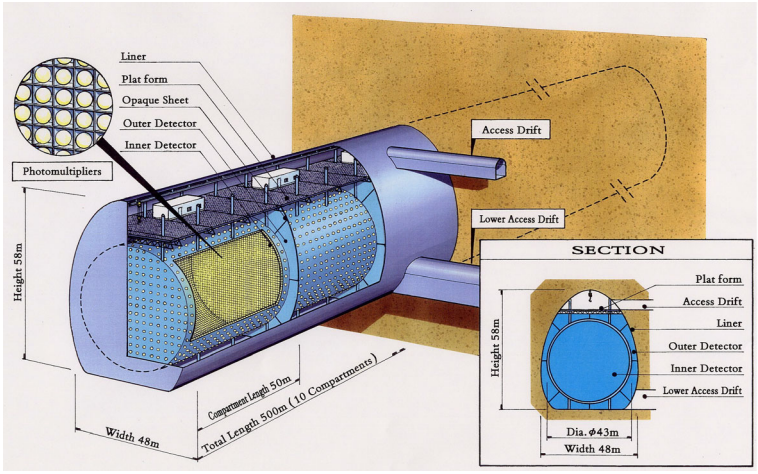

Figure 13: Schematic view of the Hyper-Kamiokande detector.

- Test of the unitarity triangle in the lepton sector
- Search for Proton decay: $p \to K^+\bar{\nu}, e^+\pi^0$

B.1 Discovery potential of CP violation in the lepton sector

If $\nu_\mu \to \nu_e$ is not observed in the first phase, another order of magnitude improvement in $\sin^2 2\theta_{\mu e}$ sensitivity to better than 10^{-3} will be performed in the second phase (Fig 10). The systematic uncertainty in background subtraction becomes important in the 2nd phase. Enhancement of the signal at the oscillation maximum and capability of measuring the background by the side-band of the oscillation pattern in the reconstructed neutrino energy distribution provide an excellent handle in controlling the systematic uncertainty.

Now that the large mixing angle solution of the solar neutrino deficit is confirmed by KamLAND, the chance of discovering CP violation is good providing that θ_{13} and δ_{CP} are not suppressed too much. The CP asymmetry is calculated as

$$A_{CP} = \frac{P(\nu_\mu \to \nu_e) - P(\bar{\nu}_\mu \to \bar{\nu}_e)}{P(\nu_\mu \to \nu_e) + P(\bar{\nu}_\mu \to \bar{\nu}_e)} = \frac{\Delta m^2_{12} L}{4E_\nu} \cdot \frac{\sin 2\theta_{12}}{\sin \theta_{13}} \cdot \sin \delta$$

By choosing a low energy neutrino beam at the oscillation maximum (E$\sim$0.75 GeV and L$\sim$295 km for JHF), CP asymmetry is enhanced as 1/E. Taking the best fit values of KamLAND, $\sin^2 2\theta_{12} = 0.91$ and $\Delta m^2_{12} = 6.9 \times 10^{-5}$, 1/10 of the CHOOZ limit for $\sin^2 2\theta_{13} = 0.01$, and $\delta = \pi/4$ (half of the maximum CP angle), A_{CP} becomes as large as 40% as shown in Figure 14. The matter effect, which creates fake CP asymmetry, increases linearly with the neutrino energy. Because of the use of low energy neutrinos, the fake asymmetry due to the matter effect is small for the JHF-Kamioka experiment.

Figure 15 shows the numbers of ν_e and $\bar{\nu}_e$ appearance events including those from backgrounds after 6 years of $\bar{\nu}_\mu$ and 2 years of ν_μ running in the 2nd phase of the JHF-Kamioka neutrino experiment. The top plot corresponds to the CHOOZ limit of $\sin^2 2\theta_{13}$=0.1 and the middle and bottom plots correspond to $\sin^2 2\theta_{13}$=0.01 and 0.001, respectively. Numbers on the plots indicates CP phase δ in degrees. CP phase at 0 degrees and 180 degrees correspond to no CP violation. 3 sigma

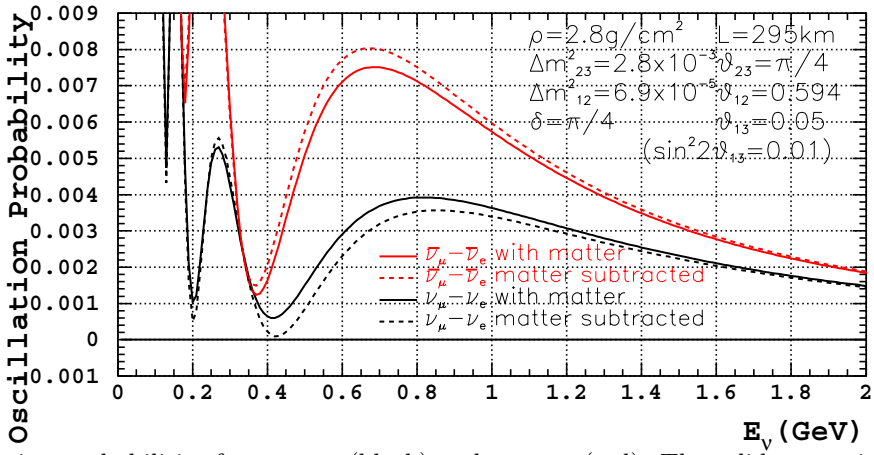

Figure 14: Oscillation probabilities for $\nu_\mu \to \nu_e$(black) and $\bar{\nu}_\mu \to \bar{\nu}_e$(red). The solid curves includes asymmetry due to matter effect. For the dashed curves, the matter effect is subtracted and the difference between $\nu_\mu \to \nu_e$(black) and $\bar{\nu}_\mu \to \bar{\nu}_e$(red) are all due to CP effect.

discovery is possible for $|\delta| > 20^\circ$ for $\sin^2 2\theta_{13}$ >0.01. There is a significant CP sensitivity left even at $\sin^2 2\theta_{13}$=0.001.

Figure 16 shows the contributions of each of the terms in $\nu_\mu \to \nu_e$ appearance for $\sin^2 2\theta_{13}$=0.01 and 0.001. Interestingly, CP violating contribution provides the largest contribution in the case of $\sin^2 2\theta_{13}$=0.001. Because the contributions of these terms are all significant, each of the components in Eq (14) could be determined by measuring the oscillation pattern of the $\nu_\mu \to \nu_e$ and $\bar{\nu}_\mu \to \bar{\nu}_e$ appearances. This oscillation pattern provides 4 independent measurements of the MNS matrix elements and can over-constrain the unitary triangle: $U^*_{e1}U_{\mu 1} + U^*_{e2}U_{\mu 2} + U^*_{e3}U_{\mu 3} = 0$ [21].

B.2 Sensitivity of proton decay

The existence of the neutrino oscillation indicates extremely small neutrino masses which are 12-13 orders of magnitude smaller than the top quark mass. A natural way to explain this hierarchy is Grand Unified theories (with see-saw mechanism), which is also indicated by the running gauge coupling constants. The only known way to directly observe the grand unification phenomenon is a nucleon decay measurement. The main gauge-boson-mediated decay is $p \to e^+\pi^0$ and the predicted lifetime could be as short as $\sim 10^{35}$ years [22]. For supersymmetric grand unified theories, $p \to \bar{\nu}K^+$ decay tends to be the main decay mode and its predicted life time is somewhere between $10^{32} - 10^{35}$ years, although this decay mode is highly model dependent. For both of these modes, it is highly desirable to reach a sensitivity of $\sim 10^{35}$ years and beyond. Current lower limits on partial lifetimes of these two modes from 92 kton-year of Super-Kamiokande data [23] are

$$\tau_p/B_{p\to e^+\pi^0} > 5.7 \times 10^{33} \text{ years (90\% confidence level)}$$

$$\tau_p/B_{p\to \bar{\nu}K^+} > 2.0 \times 10^{33} \text{ years (90\% confidence level)}$$

where τ_p is the proton lifetime and B is the branching ratio of the decay mode.

In the following sensitivity study [24], the neutrino interaction simulation and detector simulation used in Super-Kamiokande are used. Figure 17 shows simulated atmospheric neutrino backgrounds for 20 Mt·year exposure. The solid box shows the signal region used in Super-Kamiokande [25]. An estimated number of background events is 45 for 20 Mt·year, and it appears that background limits the statistics in the future $p \to e^+\pi^0$ search and so a tighter cut is desired.

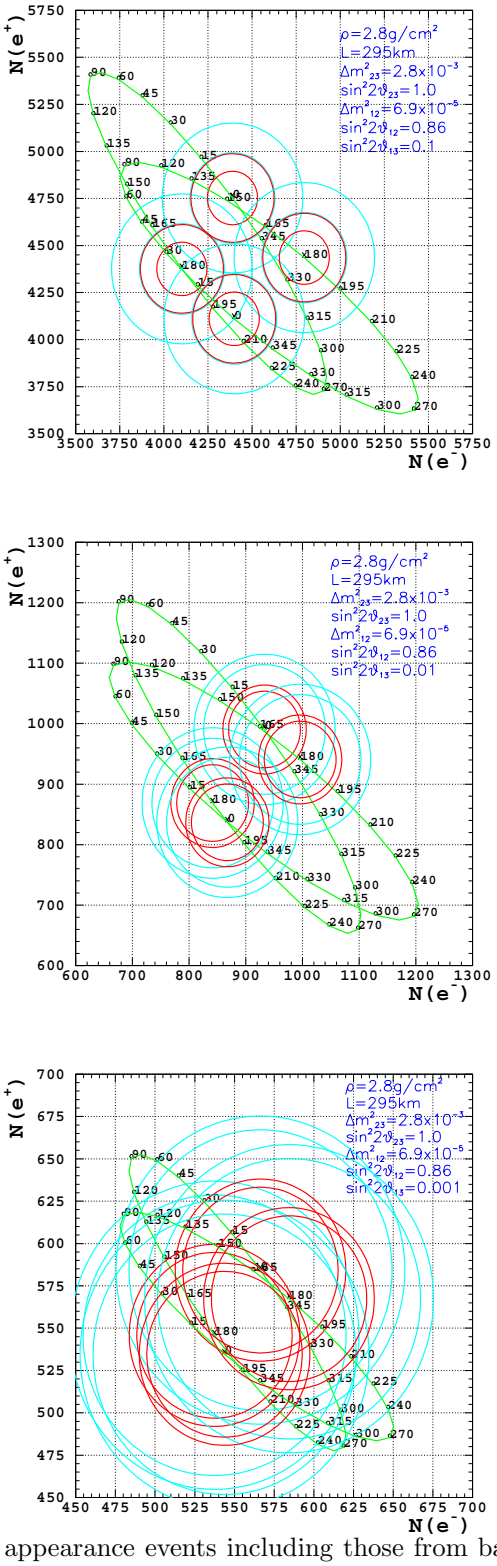

Figure 15: Numbers of ν_e and $\bar{\nu}_e$ appearance events including those from backgrounds for $\sin^2 2\theta_{13}$=0.1,0.01, and 0.001. Each of the two green contours corresponds to the different mass hierarchy and the numbers on the contour are the CP phase in degree. The red circles corresponds to the 90% contours and the blue circles are the 3σ contours after 2 years of ν_μ and 6 years of $\bar{\nu}$ runs. The outer circles includes errors due to 2% systematic uncertainty.

In the water molecule, 2 out of 10 protons are free protons. These free protons have no Fermi motion and thus give sharp proton mass peak in $e^+\pi^0$ invariant mass distribution (x-axis) and nearly perfect momentum balance (y-axis). The detection efficiency is also higher because of no pion

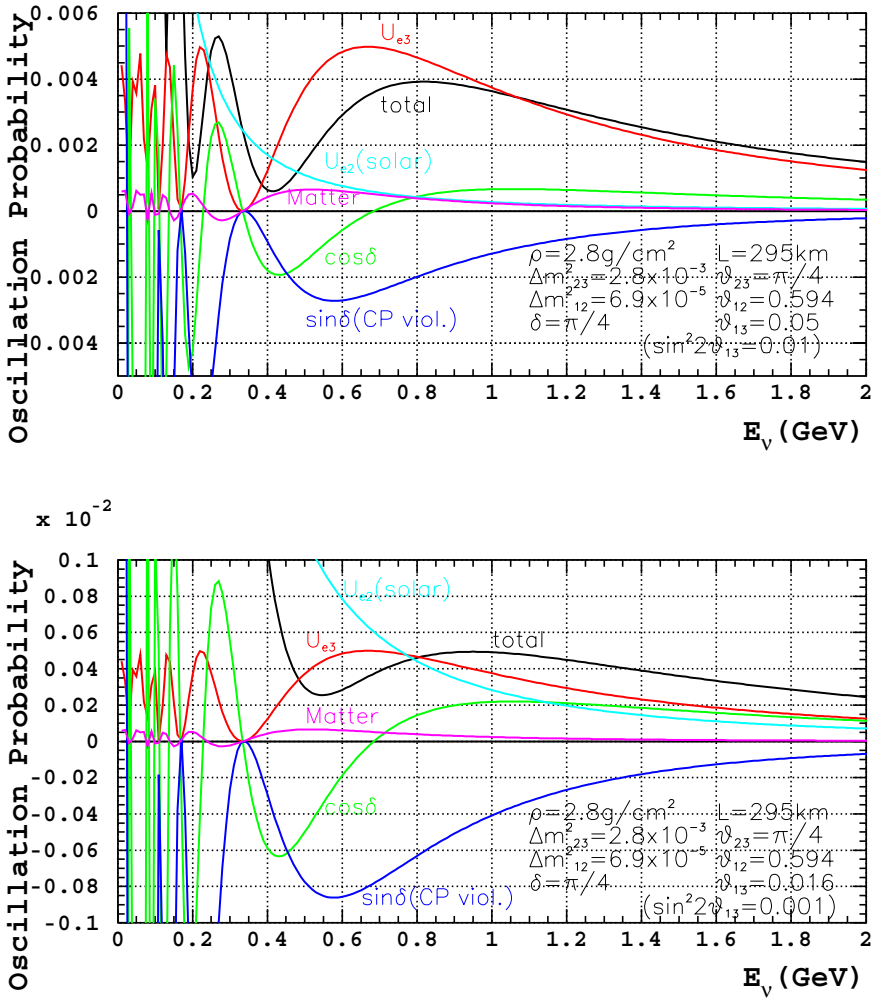

Figure 16: Contribution of different component to $\nu_\mu \to \nu_e$ appearance $\sin^2 2\theta_{13}$=0.01 and 0.001.

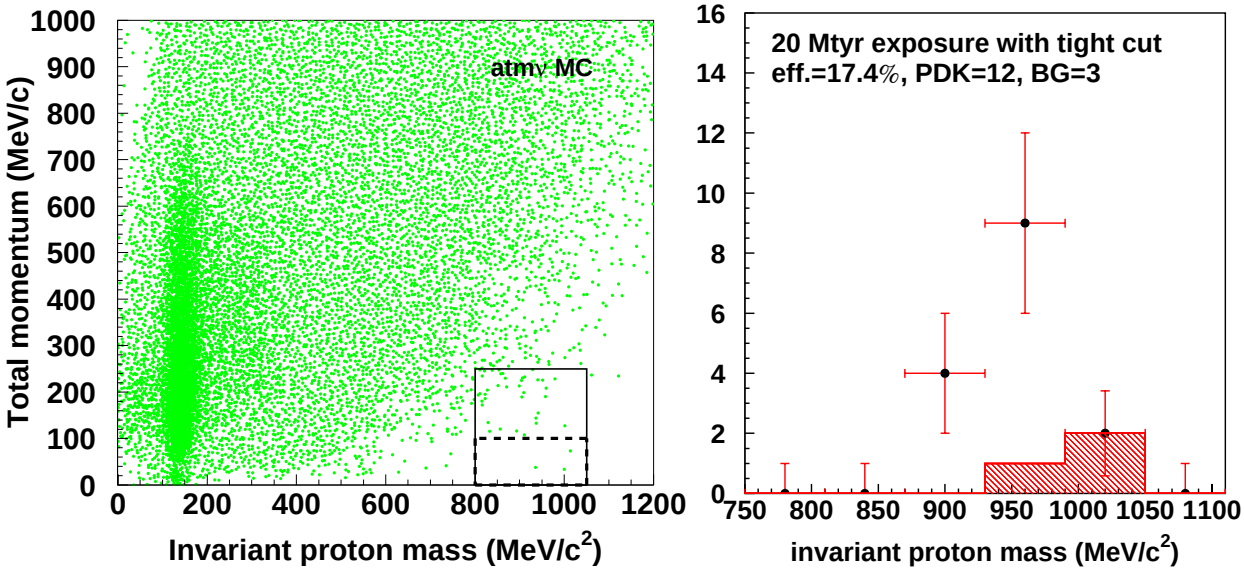

Figure 17: Left: Observed invariant proton mass and total momentum distributions for simulated atmospheric neutrino backgrounds of 20 Mt·year exposure. The solid box shows traditional selection criterion used in Super-Kamiokande [25]. Dashed box shows new tighter cut for reducing background. Right: Observed invariant proton mass distributions for 20 Mt·year exposure. Partial proton lifetime for $p \to e^+\pi^0$ is assumed to be 1×10^{35} years.

interaction loss in the oxygen nucleus. The dashed box in the figure represents a tighter selection

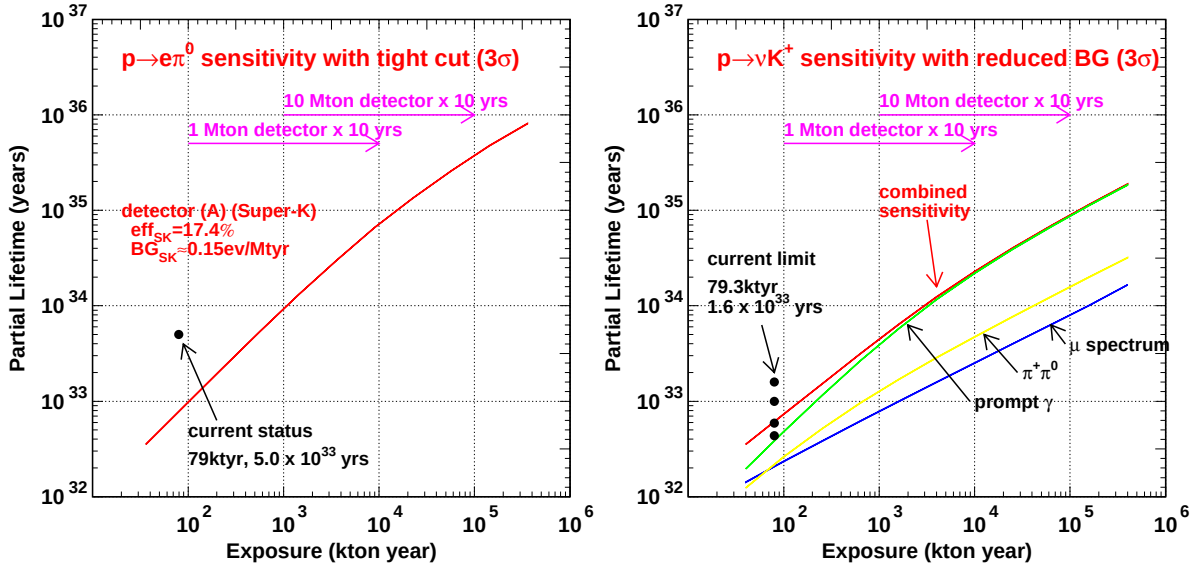

Figure 18: Expected sensitivity for the partial lifetime of protons as a function of detector exposure. In the left figure, the sensitivity for $p \to e^+\pi^0$ is calculated at 99.73%(3σ) confidence level. The tight momentum cut (see text) is used in the calculation. The right figure shows the expected sensitivity for $p \to \bar{\nu}K^+$ mode. The upper line shows the combined sensitivity for this decay mode.

criterion in momentum balance to select only the free proton decay. The background level is reduced by a factor of 15, or 3 background events/20 Mt·year, whereas 39% of the signal detection efficiency is maintained. The overall signal detection efficiency is 17.4%. Figure 17(right) shows the expected invariant mass distribution for 20 Mt·year exposure data, assuming a partial lifetime for the proton of 1×10^{35} years and the tight cut described above. A sharp peak at the proton mass is seen, which would provide a redundant positive evidence of proton decay. Figure 18(left) shows 99.73%(3σ) discovery sensitivity. With 20 Mt·year exposure, we will reach a sensitivity beyond 10^{35}years.

For the $p \to \bar{\nu}K^+$ search, Super-Kamiokande developed a nearly background free method of detecting μ^+ from a $K \to \mu\nu$ decay accompanied by a prompt γ from the residual oxygen nucleus [26]. The backgrounds for this prompt γ tagging is assumed to come from kaon production by atmospheric neutrinos. Figure 18(right) shows 99.73%(3σ) discovery sensitivity for the $p \to \bar{\nu}K^+$ search. With 20 Mt·year exposure, we will reach a sensitivity of $(2 \sim 3) \times 10^{34}$ years, closing (or opening?) the windows for many of the supersymmetric grand unified theories.

References

[1] R.H. Frampton, S.L. Glashow, T. Yanagida hep-ph/0208157

[2] High Energy News vol.21, No.3, p88 (Japanese)

[3] Y. Itow et.al. The JHF-Kamioka neutrino Project hep-ex/0106019

[4] Z. Maki, M. Nakagawa, S.Sakata, Prog. Theor. Phys. 28,870 (1962)

[5] M.Kobayashi, T. Maskawa, Proog. Theor. Phys. 49,652 (1973)

[6] Super-Kamiokande collaboration, Phys.Rev.Lett. 81,1562 (1998)

[7] K2K collaboration, hep-ex/0212007, accepted for publication in Phys.Rev.Lett.

[8] Super-Kamiokande collaboration, Phys.Rev.Lett.85,3999 (2000)

[9] SNO Collaboration, Phys.Rev.Lett.89,011301(2002)

[10] The Super-Kamiokande collaboration, Phys. Rev. Lett.86,5651 (2001), Phyys. Rev. Lett.86,5656 (2001)

[11] KamLAND Collaboration. hep-ex/0212021

[12] For example, Yamanoi Y. et al., KEK Preprint 97-225, November 1997.

[13] D. Beavis, A. Carroll, I. Chiang, *et al.*, Proposal of BNL AGS E-889 (1995).

[14] R. Brun et al., CERN DD/EE/84-1 (1987).

[15] T.A.Gabriel et al., ORNL/TM-11185; C.Zeitnitz and T.A.Gabriel, Nucl. Instr. and Meth. **A349**, 106 (1994).

[16] K. Nishikawa, talk presented at KEK-PS review, Dec., 2000; T. Nakaya, talk presented at 2001 Lake Louise Winter Institute, Feb., 2001.

[17] CHOOZ: Apollonio M. et al., Phys. Lett. **B**466 (B1999) 415. Palo Verde:F. Boehm *et al.*, Nucl.Phys.Proc.Suppl. 91:91(2001)

[18] B. Richter, SLAC-PUB-8587 (hep-ph/0008222), 2000 and references there in.

[19] M. Furusaka, R. Hino, Y. Ikeda *et al.*, *"The Joint Project for High-Intensity Proton Accelerators"*, KEK Report 99-4; JAERI-Tech 99-056; JHF-99-3 (1999).

[20] M. Koshiba, *Phys. Rep.* **220**, 229 (1992); K. Nakamura, talk presented at Int. Workshop on Next Generation Nucleon Decay and Neutrino Detector, 1999, SUNY at Stony Brook; K. Nakamura, *Neutrino Oscillations and Their Origin*, (Universal Academy Press, Tokyo, 2000), p. 359.

[21] J. Sato, hep-ph/0008056 (2000).

[22] W. Marciano, talk presented at UNO proto-collaboration meeting, 2000, Carlsbad, USA.

[23] M. Shiozawa, talk presented at the 30th Int. Conf. on High Energy Physics (ICHEP2000), 2000, Osaka, Japan.

[24] M. Shiozawa, *Next Generation Nucleon Decay and Neutrino Detector(NNN99)* (AIP Conference Proceedings 533, AIP, New York, 2000) p.21; M. Shiozawa, talk presented at Int. Workshop on Next Generation Nucleon Decay and Neutrino Detector, 2000, Fermi National Laboratory, USA.

[25] M. Shiozawa *et al.*, *Phys. Rev. Lett.* **81**, 3319 (1998).

[26] Y. Totsuka, *7th Workshop on Grand Unification, ICOBAN '86*, (World Scientific, 1986), p. 118; Y. Hayato *et al.*, *Phys. Rev. Lett.* **83**, 1529 (1999).